
No. _____

SUPREME COURT OF THE UNITED STATES

THOMAS STALCUP,

Applicant,

v.

DEPARTMENT OF DEFENSE AGENCY,
Office of the Secretary of Defense of the United States,

Respondent.

EXHIBIT 1

Thomas F. Stalcup
961 Kent Lane
Palm Harbor, FL 34683
(774) 392-0856
stalcupt@gmail.com

Thomas F. Stalcup, PhD
Pro Se Litigant

United States Court of Appeals For the First Circuit

No. 22-1405

THOMAS STALCUP,

Plaintiff - Appellant,

v.

DEPARTMENT OF DEFENSE AGENCY, Office of the Secretary of Defense of the United
States,

Defendant - Appellee.

Before

Kayatta, Lynch and Montecalvo,
Circuit Judges.

ORDER OF COURT

Entered: June 5, 2023

Plaintiff-appellant's motion for an injunction and temporary restraining order against the National Transportation Safety Board ("NTSB") is denied, as it seeks relief far beyond the scope of this appeal.

By the Court:

Maria R. Hamilton, Clerk

cc:

Thomas Stalcup

Donald Campbell Lockhart

Rayford A. Farquhar

Michael L. Fitzgerald

No. _____

SUPREME COURT OF THE UNITED STATES

THOMAS STALCUP,

Applicant,

v.

DEPARTMENT OF DEFENSE AGENCY,
Office of the Secretary of Defense of the United States,

Respondent.

EXHIBIT 2

Thomas F. Stalcup
961 Kent Lane
Palm Harbor, FL 34683
(774) 392-0856
stalcupt@gmail.com

Thomas F. Stalcup, PhD
Pro Se Litigant

UNITED STATES DISTRICT COURT
FOR THE DISTRICT OF MASSACHUSETTS

CIVIL ACTION
NO. 1:22-cv-11032-AK

KRICK et. al.,)
)
Plaintiffs)
)
vs.)
)
RAYTHEON COMPANY et. al.,)
)
Defendants)

AFFIDAVIT OF THOMAS F. STALCUP, PHD

1. My name is Thomas F. Stalcup. I am a US citizen and hold PhD in physics.
2. I have visually inspected the wreckage of TWA Flight 800, and I am familiar with the National Transportation Safety Board (NTSB) crash sequence for TWA Flight 800, as well as where certain wreckage items are located on the aircraft reconstruction.
3. I have also reviewed thousands of pages of NTSB materials on this crash, and I am familiar with various, respective bodies of evidence, including aircraft damage patterns, radar information, the debris field distribution of wreckage, and the results of NTSB studies and reports relevant to the Plaintiffs' claims.
4. Regarding the debris field distribution of wreckage, I have reviewed the NTSB's "red zone" debris field database from this incident, which comprises wreckage items recovered closest to JFK Airport and includes parts that left the aircraft soon after the initiating event. The NTSB concluded that the items that landed in the red zone exited the aircraft after an explosion that caused the aircraft to break in half in midair.

5. The forward section of the plane, including the cockpit, landed in the “yellow zone”, which was further along the flight path than the red zone. The rear section, with the wings, continued even further, landing in the furthest debris field, known as the “green zone”.
6. Many wreckage items that the NTSB determined landed in the red zone were from a section of the aircraft fuselage just forward of the wings. One such item from this section was labeled LF-24A.

**Part LF-24A Was Recently Discovered To Have Been Altered
After Being Recovered From The Ocean**

7. LF-24A is a part that mates with both red and yellow zone parts.
8. Exhibit A contains a true and correct copy of official NTSB notes for LF-24A from that agency's investigation, which describes a 180 degree inboard curl. Exhibit A also includes true and correct copies of official NTSB photos of LF-24A, taken prior to being placed onto the reconstruction. These photos show the 180 degree inboard curl.
9. As a consultant for the Plaintiffs in this action, I visited the reconstruction of the TWA Flight 800 aircraft on January 26, 2023. A high priority for this inspection was to view the red zone parts, including part LF-24A with its inboard curl.
10. I attempted, but failed to locate part LF-24A during that visit.
11. Later, when reviewing photographs from that visit in my office, I located part LF-24A. It no longer had its inboard curl. It had been flattened.
12. Part LF-24A's current, flattened state is a major reason why I did not locate or recognize this part in the reconstruction during the inspection.
13. Exhibit B contains two copies (Figures 1 and 2) of a photo of part LF-24A and other nearby parts on the lower left side of the fuselage, which was taken during my most recent

visit to the reconstruction on behalf of the Plaintiffs. Figure 1 in Exhibit B is a true and correct copy of this photo. Figure 2 in Exhibit B is a copy of this photo with parts adjacent to LF-24A darkened to more clearly depict part LF-24A.

14. A white triangle in the corner of LF-24A is visible in this photo, which was taken from below the aircraft reconstruction. This triangle would not be visible in this photo if the part retained its original 180 degree inboard curl (see Exhibit A). Instead, it would be visible from above this part, from within the adjacent cargo bay.
15. Based on LF-24A's current condition, it appears as though some person or persons bent it approximately 180 degrees. This manipulation made that section of the fuselage more closely resemble its condition prior to suffering damage during the crash.

**NTSB Analyses Of “Red Rusty” Metal Particles Inside The
TWA Flight 800 Reconstruction May Be Incomplete And Unavailable**

16. Salt water hastens the rusting (oxidation) of metal. See, for example:
<https://www.vedantu.com/question-answer/effect-does-salt-have-on-the-corrosion-of-iron-class-12-chemistry-cbse-60ed1639ce33ce53523b916d> (“Salt, or more particularly, salt solution, can hasten the rusting process by acting as an electrolyte, allowing the metal (iron) to lose electrons more quickly. Rusting is caused by a chemical process called as oxidation, in which metal atoms lose electrons and produce ions”).
17. When ferrous metals such as iron or steel rusts, it turns red or orange in color. “The development of iron oxides, which is known as rusting, is an example of electrochemical corrosion. This sort of damage causes the original metal to generate oxides or salts, resulting in a unique orange coloration.” Id.

18. The center wing tank of a 747 is made primarily out of aluminum. A smaller percentage of the total aircraft components, by volume and weight, is made from specific steel alloys. When aluminum oxidizes, it does not turn red or orange. It turns white. Results from a Google search for the “color of aluminum oxide” can confirm this.
19. Various missile warheads are encased in a steel shell and/or surrounded by preformed steel fragments. The specific steel alloys used in these warheads are known by missile manufacturers and designers.
20. Upon detonation, a warhead's casing and/or its preformed fragments break apart, and the forces from that detonation, by design, send some of the broken metal fragments toward a target. These fragment can penetrate or otherwise enter the target. See, e.g., Exhibit C, which is a true and correct copy of the “Hal.Science” website's article entitled “Fragment mass distribution of metal cased explosive charges”.
21. Steel fragments from a warhead casing can contain a significant amount of iron and turn red or orange as as they rust.
22. Most or all center wing tank parts were immersed in salt water for days or weeks before being recovered, which could have hastened any such oxidation.
23. Small metal particles were found embedded into the sealant of the ceiling of the center wing tank.
24. This section of the tank's ceiling is also directly above an upward bulge and fractures in the tank's floor.
25. The floor's upward bulge and fractures, together with the particles being embedded in the ceiling of the tank are consistent with these particles having upward-trajectories.

26. Such trajectories, together with the original 180 degree inboard curl of part LF-24A, are consistent with the detonation of a missile warhead a distance below the aircraft.
27. Certain of these particles were described by NTSB investigator(s) as being “rusted red” in color, indicating that they are steel.
28. Exhibit D is a true and correct copy of the NTSB's “Metal Particle Summary” from the TWA Flight 800 investigation, which contains hand-written descriptions by one or more NTSB investigators of some of these metal particles, which appear to have included both steel and aluminum particles.
29. One or more of these particles appear to have been broken from from identified aircraft components. Other particles do not appear to have been identified by the NTSB.
30. On page eight (8) of this report, four particles or areas are described as “red rusty”, indicating that the objects responsible for the discoloration were likely steel, and not aluminum.
31. The NTSB noted that one such “red rusty” particle was removed by an NTSB investigator on December 5, 1996. See “Metal Particle Summary” at 8, Exhibit 4.
32. NTSB Fire and Explosion Report No. 20A indicated that the metal particles removed by the NTSB from the tank's upper sealant were analyzed and that findings from these analyses are available in Appendix III of that report (“Appendix III contains the findings of the analysis of the metal debris removed from the sealant in the center wing tank.”). The government provided a hyperlink to that report (<https://data.nts.gov/Docket/?NTSBNumber=DCA96MA070>) in its motion to dismiss, D.74, p.2, n.1.

33. However, Appendix III of that Fire and Explosions Group Exhibit available at the same government-provided hyperlink does not contain these findings, but instead lists as “Pending”, the “Description of Material embedded in CWT upper skin sealant.” See “Fire and Explosion 20 - Exhibit No. 20C - Appendix III (Tests and Study)”. Id.
34. Metallurgists and various commercial companies (e.g., <https://forcetechnology.com/en/services/materials/analysis-steel-metals>) can analyze metal particles to determine the specific alloy from which they were forged. After such an analysis, investigators can cross-reference the resultant alloy to determine if a respective particle is consistent with a specific metal alloy used in missile casings or from an alloy of aluminum or steel used in 747 airliners.
35. The NTSB has apparently not released any such analyses, cross references, or comparisons of these metal particles.
36. The Plaintiffs may be able to retrieve any remaining such particles and analyze them.
37. Analyses of these particles could indicate or show that one or more of them were from a warhead casing, which would help the Plaintiffs prove their case.

I hereby declare under the pains and penalties of perjury that the foregoing is true and correct to the best of my knowledge, information, and belief.

Signature: THOMAS STALCUP

Date: 6/19/2023

Name: Thomas Stalcup, PhD

No. _____

SUPREME COURT OF THE UNITED STATES

THOMAS STALCUP,

Applicant,

v.

DEPARTMENT OF DEFENSE AGENCY,
Office of the Secretary of Defense of the United States,

Respondent.

EXHIBIT 3

Thomas F. Stalcup
961 Kent Lane
Palm Harbor, FL 34683
(774) 392-0856
stalcupt@gmail.com

Thomas F. Stalcup, PhD
Pro Se Litigant

UNITED STATES DISTRICT COURT
FOR THE DISTRICT OF MASSACHUSETTS

CIVIL ACTION
NO. 1:22-cv-11032-AK

KRICK et. al.,)
 Plaintiffs)
))
vs.)
))
RAYTHEON COMPANY et. al.,)
 Defendants)

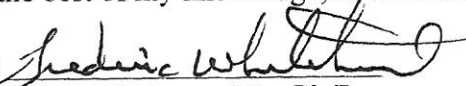
AFFIDAVIT OF FREDERIC WHITEHURST, J.D., Ph.D

1. I am Dr. Frederic Whitehurst, J.D., Ph.D.. I am an Attorney at Law as well as a forensic consultant.
2. I hold a BS in Chemistry (1974) from East Carolina University, a Ph.D. in Chemistry (1980) from Duke University, spent two years as a post-doctoral research fellow at Texas A&M University and hold a J.D. (1996) from Georgetown University.
3. I practice law in North Carolina and also consult in matters involving analytical chemistry throughout the United States.
4. I was employed as a Special Agent of the federal bureau of investigation from 1982 until 1998. I was attached to the FBI crime laboratory from 1986 until 1998.
5. My area of expertise at the FBI laboratory was in analytical chemistry of materials from bombing crime scenes. During that time I worked about one thousand cases, mostly involving explosives related matters.
6. As a result of my education as well as my experience in the FBI crime laboratory I offer the following concerning analysis of explosives residues:

7. Following initiation of energetic materials causing explosions often residues of either the original explosives used or reaction products of the explosive chemical reactions adhere to surfaces in the vicinity of the site of the explosions.
8. Due to the chaotic nature of explosions predicting which objects will have residues upon them is simply at best guess work and/or like hunting for a particle of sand on a beach. For instance, one might expect to find residues on items that were in close proximity to the explosion and yet due to the thermal environment such residues may totally react leaving no residue.
9. Another factor controlling where one might find residues is the environments in which an object is found. For instance, aqueous environments might very well dissolve water soluble explosives components and residues. Examples of such environments would include water from firefighting efforts as well as objects retrieved from under water.
10. Residues might also be identified on evidence that did not originate from bombings simply due to contamination issues with instrumentation and glassware within a crime laboratory.
11. Residues adhere to outer surfaces of objects but also in the situation where plastic and rubber materials are retrieved residues may very well be found inside the matrices of those materials. Retrieval would require submersion of evidence in appropriate solvents followed by ultrasound bath, collection of the solvent/possible residue, and analysis of that solution.
12. I am aware of “splatter” deposits that were found on various TWA Flight 800 wreckage items, which were found to contain nitrates. This splatter material appeared to be melted polyurethane foam, which resolidified on metal surfaces. This material may be a good candidate for the retrieval of any potential explosive residues inside its matrices using the

technique I described above. It would be advisable to preserve wreckage items with an adequate amount of splatter material for such analysis.

I hereby declare under the pains and penalties of perjury that the foregoing is true and correct to the best of my knowledge, information, and belief.

Signature: 
Name: Frederic Whitehurst, J.D., Ph.D

No. _____

SUPREME COURT OF THE UNITED STATES

THOMAS STALCUP,

Applicant,

v.

DEPARTMENT OF DEFENSE AGENCY,
Office of the Secretary of Defense of the United States,

Respondent.

EXHIBIT 4

Thomas F. Stalcup
961 Kent Lane
Palm Harbor, FL 34683
(774) 392-0856
stalcupt@gmail.com

Thomas F. Stalcup, PhD
Pro Se Litigant

No. _____

SUPREME COURT OF THE UNITED STATES

THOMAS STALCUP,

Applicant,

v.

DEPARTMENT OF DEFENSE AGENCY,
Office of the Secretary of Defense of the United States,

Respondent.

ORDER for Stay or Injunction Pending the Filing and Disposition of a
Writ of Certiorari to the United States
Court of Appeals for the First Circuit

BY The Honorable Ketanji Brown Jackson,
Circuit Justice for the First Circuit

Applicant Stalcup's motion for a Stay or Injunction is GRANTED and it is hereby ORDERED that the National Transportation Safety Board ('NTSB') shall preserve the following four aircraft components pending the filing and disposition of the respective writ of certiorari to the United States Court of Appeals for the First Circuit: CW-102, CW-114, CW-148, and CW-129.

BY The Honorable Ketanji Brown Jackson, Circuit Justice for the First Circuit on this _____ day of July, 2023.

No. _____

SUPREME COURT OF THE UNITED STATES

THOMAS STALCUP,

Applicant,

v.

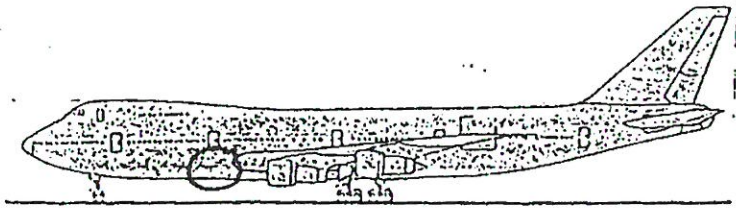
DEPARTMENT OF DEFENSE AGENCY,
Office of the Secretary of Defense of the United States,

Respondent.

EXHIBIT A

Thomas F. Stalcup
961 Kent Lane
Palm Harbor, FL 34683
(774) 392-0856
stalcup@gmail.com

Thomas F. Stalcup, PhD
Pro Se Litigant



LOG # LF24 ⁵⁰⁹ ¹²⁵ 10-7-92

TARGET # LLS 369

COORD: LAT 40-38-26.

LONG 72-38-34.1

DEBRIS FIELD #3 (near)
Red

- (A) No I.D.
- (B) Red Tag # A752

Two belly skin panels adjacent to the belly skin panel identified as LFB.

Panel (A)

This panel shares a fracture surface with LFB. No frames remain. 2 bays of s-40 remain. No obvious signs of burning or soot. Panel is curled inbd as indicated.

Panel (B)

Most of stringers 38 and 39 remain attached. No frames. No obvious signs of burning or sooting.

REFER METALLURGY GROUP NOTES

REFER FIRE AND EXPLOSION GROUP NOTES FOR FIRE DAMAGE

S. Chisholm
8/11/96

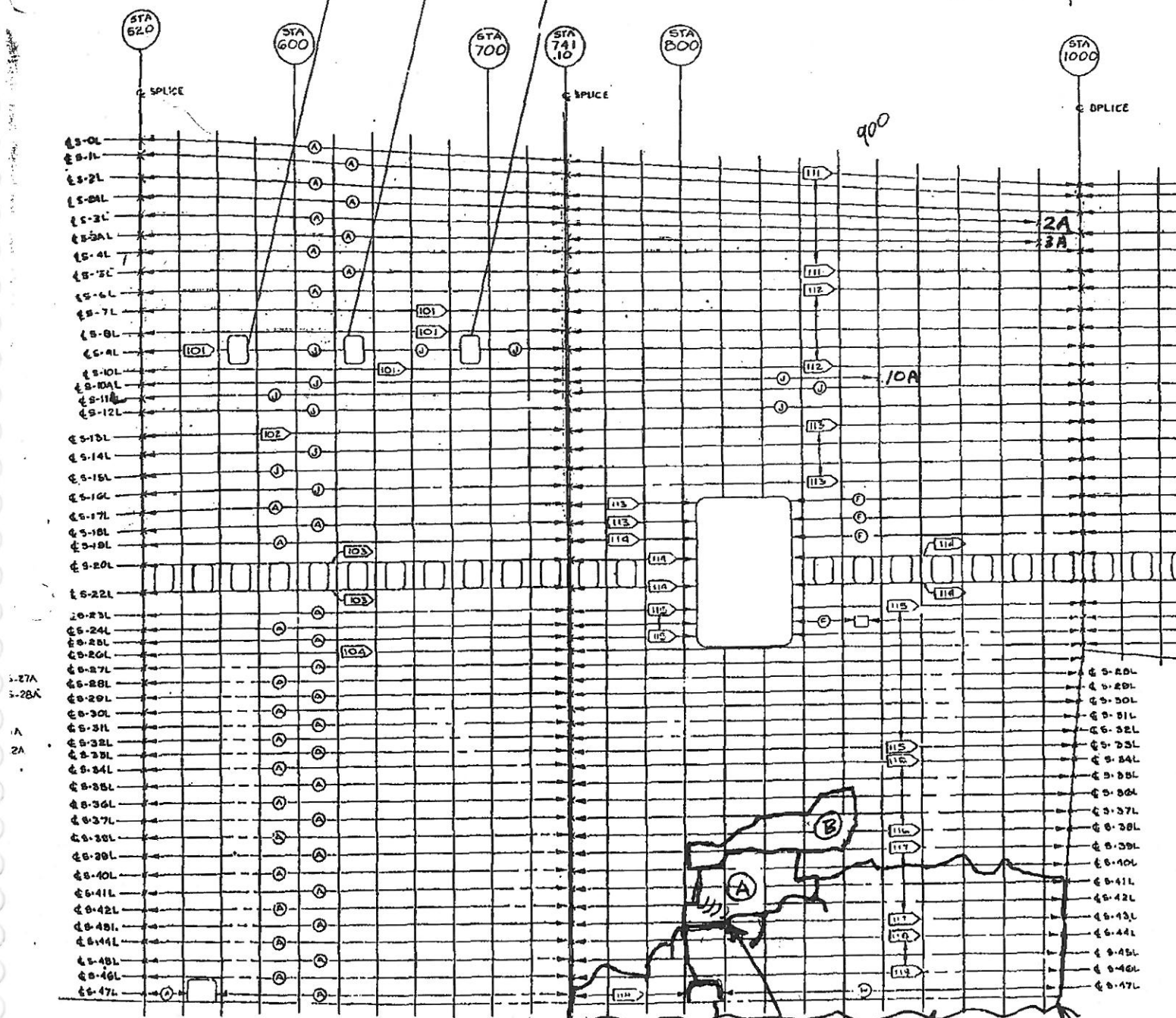
Nail Scoville
TWA-10-6-96
Stephen F. Klupach Jr
FBI 10-22-96
R. Brubaker
IAM 10-25-96

LF 24

1 SEC 42

SEC 42 | SEC 4

SEE 65B00004



Panel A
curled
in bnd 1800

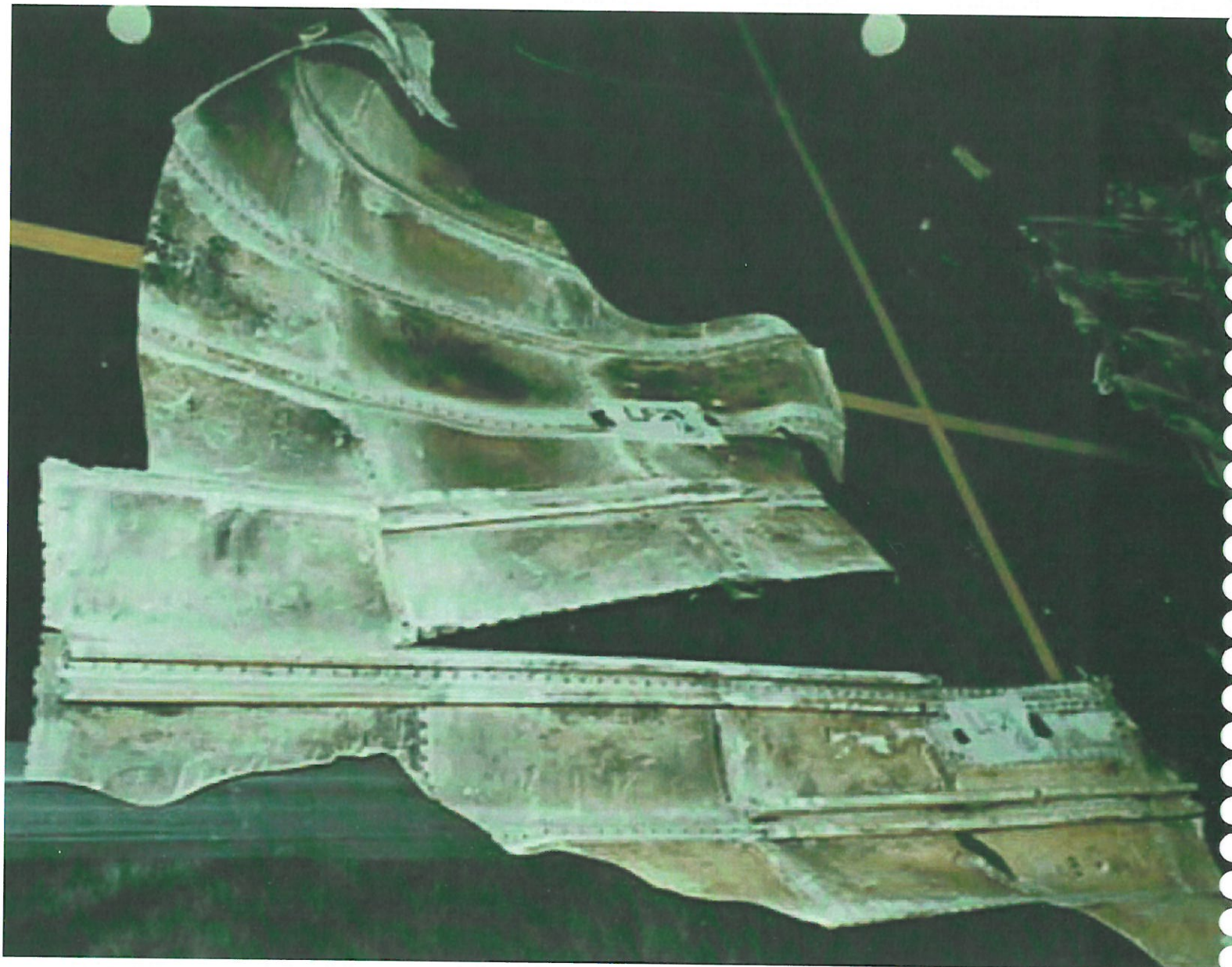
STA 800.00

FRON SPAI

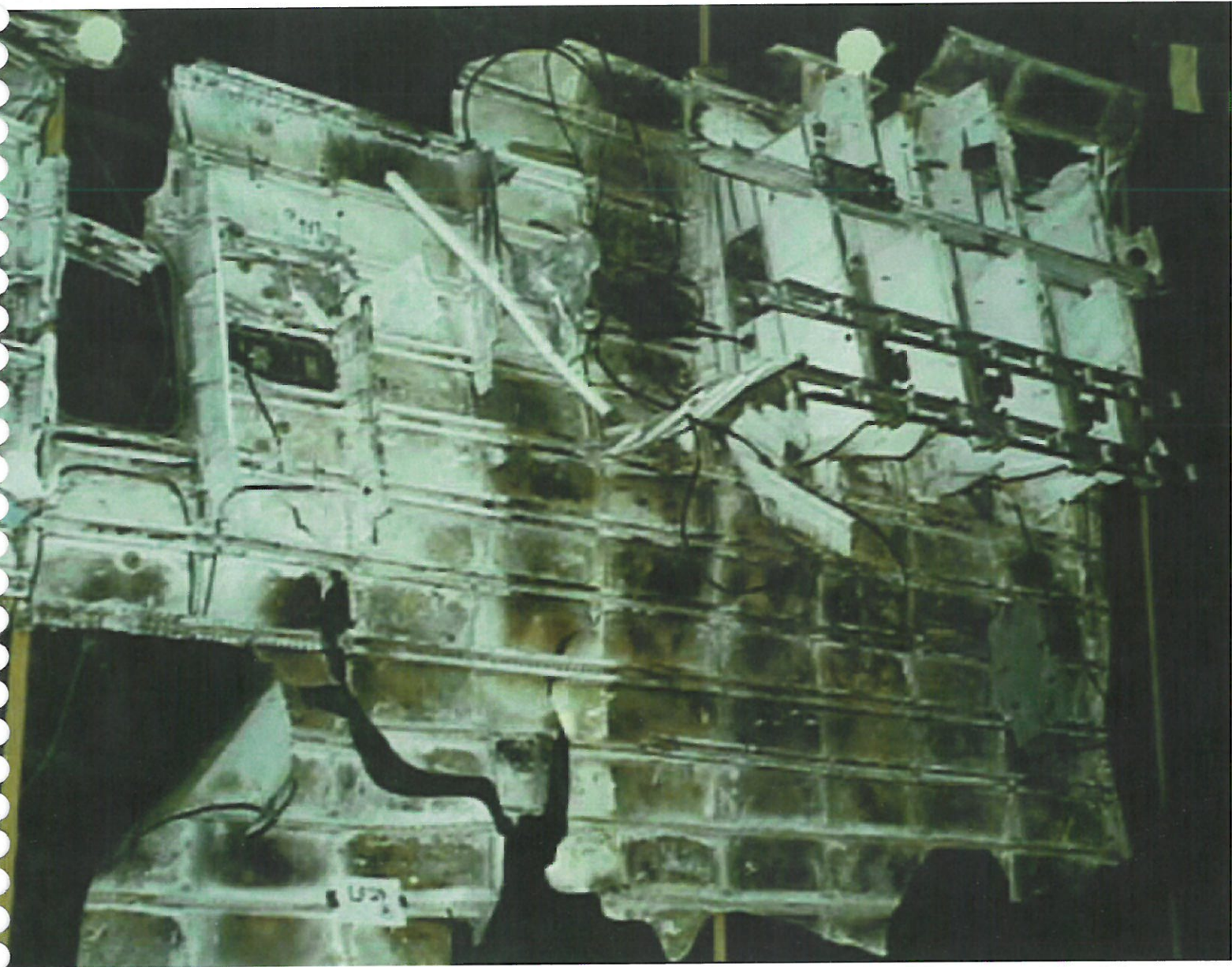
65B0000513

Stephen F. Klupach Sr
FAN 10-22-96

2



Structures 7 - LF24 - Photo 1



Structures 7 - LF24 - Photo 2

No. _____

SUPREME COURT OF THE UNITED STATES

THOMAS STALCUP,

Applicant,

v.

DEPARTMENT OF DEFENSE AGENCY,
Office of the Secretary of Defense of the United States,

Respondent.

EXHIBIT B

Thomas F. Stalcup
961 Kent Lane
Palm Harbor, FL 34683
(774) 392-0856
stalcup@gmail.com

Thomas F. Stalcup, PhD
Pro Se Litigant

UNITED STATES DISTRICT COURT
FOR THE DISTRICT OF MASSACHUSETTS

CIVIL ACTION
NO. 1:22-cv-11032-AK

KRICK et. al.,)
Plaintiffs)
vs.)
RAYTHEON COMPANY et. al.,)
Defendants)

EXHIBIT B

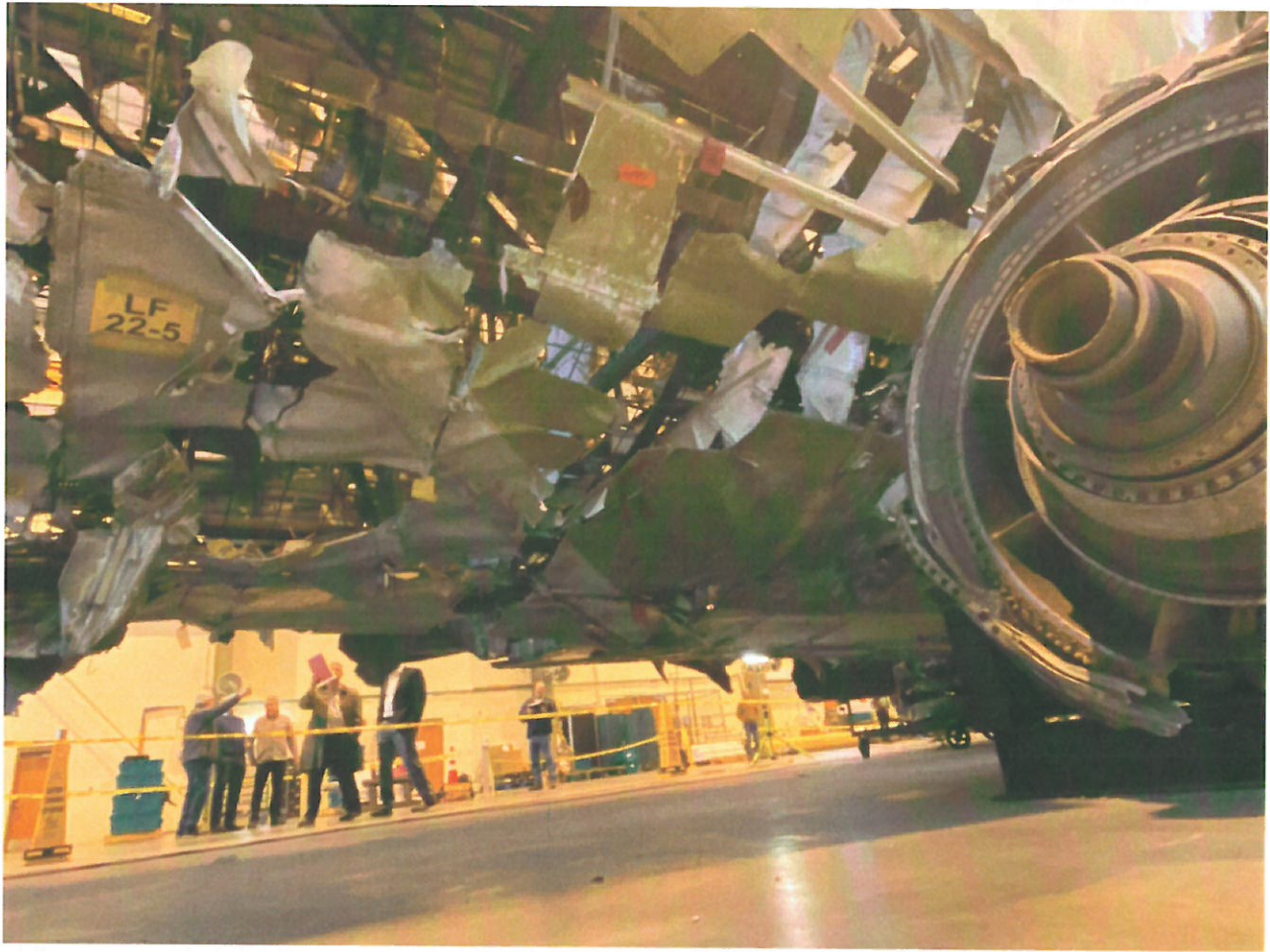


Figure 1. Photo of the lower left fuselage of the TWA Flight 800 reconstruction taken on January 26, 2023. Part LF-24A is to the left of the engine. See Figure 2 below, where part LF-24A is highlighted.

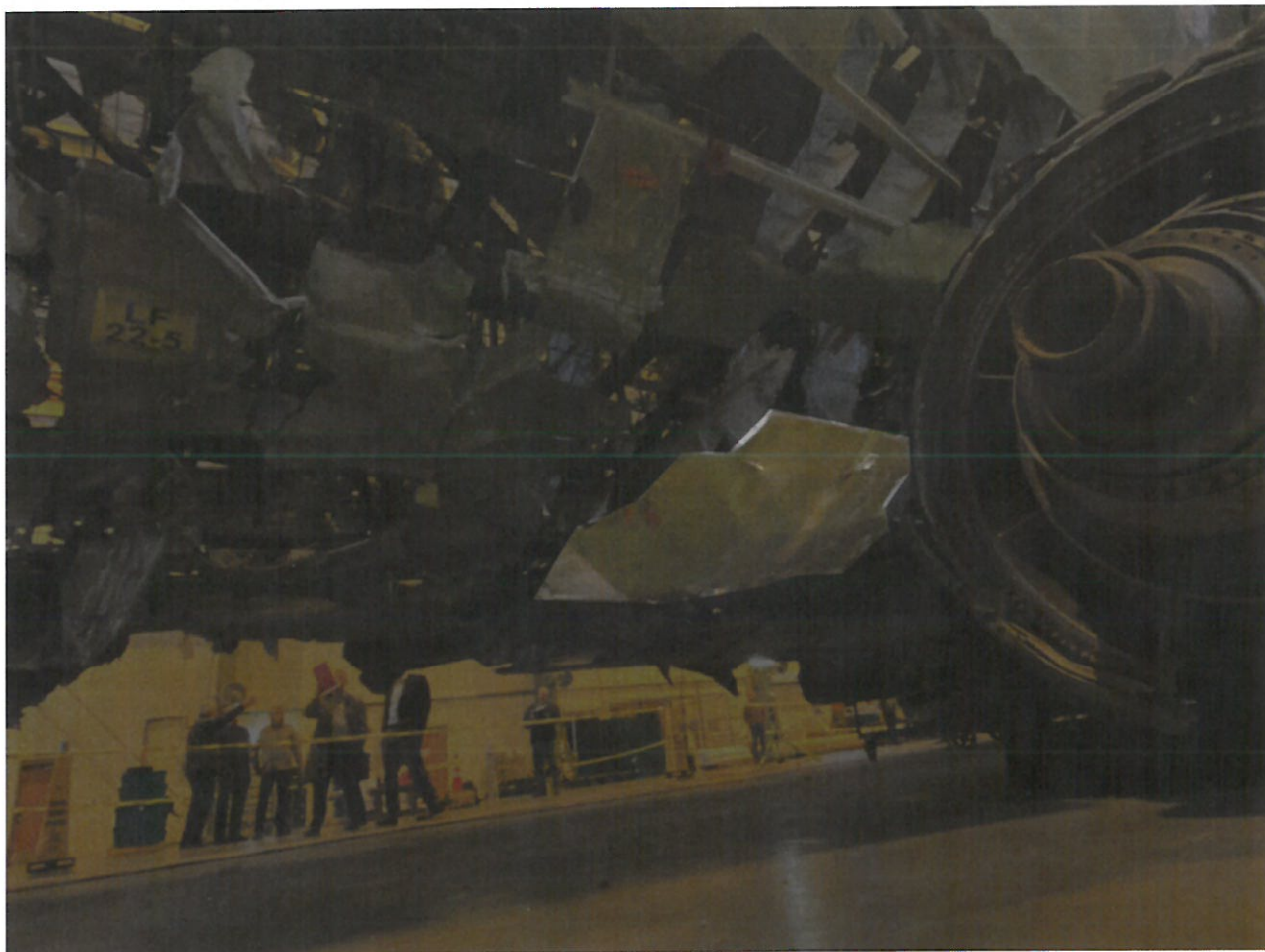


Figure 2. Photo of the lower left fuselage of the TWA Flight 800 reconstruction with all visible parts darkened except part LF-24A.

No. _____

SUPREME COURT OF THE UNITED STATES

THOMAS STALCUP,

Applicant,

v.

DEPARTMENT OF DEFENSE AGENCY,
Office of the Secretary of Defense of the United States,

Respondent.

EXHIBIT C

Thomas F. Stalcup
961 Kent Lane
Palm Harbor, FL 34683
(774) 392-0856
stalcup@gmail.com

Thomas F. Stalcup, PhD
Pro Se Litigant



HAL
open science

Fragment mass distribution of metal cased explosive charges

W. Arnold, E. Rottenkolber

► **To cite this version:**

W. Arnold, E. Rottenkolber. Fragment mass distribution of metal cased explosive charges. International Journal of Impact Engineering, 2008, 35 (12), pp.1393. 10.1016/j.ijimpeng.2008.07.049 . hal-00542565

HAL Id: hal-00542565

<https://hal.science/hal-00542565>

Submitted on 3 Dec 2010

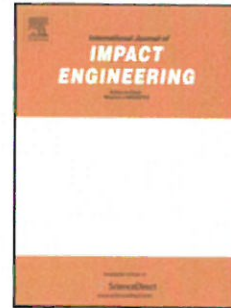
HAL is a multi-disciplinary open access archive for the deposit and dissemination of scientific research documents, whether they are published or not. The documents may come from teaching and research institutions in France or abroad, or from public or private research centers.

L'archive ouverte pluridisciplinaire **HAL**, est destinée au dépôt et à la diffusion de documents scientifiques de niveau recherche, publiés ou non, émanant des établissements d'enseignement et de recherche français ou étrangers, des laboratoires publics ou privés.

Accepted Manuscript

Title: Fragment mass distribution of metal cased explosive charges

Authors: W. Arnold, E. Rottenkolber



PII: S0734-743X(08)00169-3

DOI: [10.1016/j.ijimpeng.2008.07.049](https://doi.org/10.1016/j.ijimpeng.2008.07.049)

Reference: IE 1651

To appear in: *International Journal of Impact Engineering*

Received Date:

Revised Date:

Accepted Date:

Please cite this article as: Arnold W, Rottenkolber E. Fragment mass distribution of metal cased explosive charges, *International Journal of Impact Engineering* (2008), doi: [10.1016/j.ijimpeng.2008.07.049](https://doi.org/10.1016/j.ijimpeng.2008.07.049)

This is a PDF file of an unedited manuscript that has been accepted for publication. As a service to our customers we are providing this early version of the manuscript. The manuscript will undergo copyediting, typesetting, and review of the resulting proof before it is published in its final form. Please note that during the production process errors may be discovered which could affect the content, and all legal disclaimers that apply to the journal pertain.

Fragment mass distribution of metal cased explosive charges

W. Arnold^{*}, E. Rottenkolber^{**}

^{*}*MBDA-TDW Gesellschaft für verteidigungstechnische Wirksysteme mbH, Hagenauer Forst 27,
D-86529 Schrobenhausen, Germany*

^{**}*NUMERICS GmbH, Mozartring 6, D-85238 Petershausen, Germany*

Abstract

Fragmentation of metal casings is an important issue in a variety of problems like weapon effectiveness, safety distances or collateral damage. To be able to describe the intended or unintended effects of naturally fragmenting shells, one needs to know the mass distribution of the fragments produced after detonation of the explosive charge. In the present study the fragmentation behavior of very light and heavier casings has been investigated. The data collection method is outlined and applied to the fragment mass distribution of four different shells. The results are given in diagrams. It was found that an existing fragmentation model adequately predicts the dependence of circumferential fragment size on material strength. Fracture in axial direction should also be considered to predict correct fragment masses, but currently a suitable model for this purpose is not available.

Keywords: Fragmentation, Metal casing, Explosive charge

1. Introduction

Effects of naturally fragmenting shells are of interest under various circumstances like predicting a weapon's effectiveness or its ability to inflict collateral damage. The effects of fragments may be unintended when shaped charges or blast charges are used to defeat a target. However, for structural reasons these charges are generally equipped with thin metal casings. On the other hand heavier steel casings are used for ammunition when the fragments are the intentional effective defeat mechanism.

In the present study the fragmentation behavior of different metal casings has been studied. Light casings were made from thin Aluminum-alloy and mild steel shells. Heavier casings were made from mild steel and hard steel. The mild steel is typical for structural applications. The hard steel was tested in two conditions, namely in the annealed condition as received from the supplier and in a heat treated condition.

The data collection method is based on image processing of photographs of witness plates, where the holes pierced by impacting fragments are detected with the help of a computer program. A variant

^{*} Corresponding author. Tel.: +49 8252 996267; fax: +49 8252 996733.
E-mail address: werner.arnold@mbda-systems.com

of this method had been developed for the study of behind armor debris (BAD) clouds of steel targets caused by shaped charge jet attacks [1 to 3]. The approach used for natural fragmentation is sketched in the presented paper. The idea is to measure the hole distribution and from that to infer the mass distribution of the fragments knowing their velocity and thickness. Clearly, a couple of additional assumptions are needed to solve this problem.

The obtained mass distributions are presented within diagrams and the three different kinds of steel casings are compared. The high fragment masses produced by the hard steel casing in the annealed condition seemed to contradict not only common experience but also an existing model of circumferential fragmentation. Therefore, a closer examination is presented that finally supports the model, but also shows the need for a more general model, i.e. a model which is not restricted to circumferential fracture.

2. Experimental Study

Cylindrical explosive charges having a diameter of 100 mm and a height of 200 mm have been used for the test samples. The plastic bonded cast-cured charges were made from KS33 (= HMX/HTPB 90/10). This explosive has a density of 1.71 g/cm³ and a detonation velocity of 8480 m/s. A Gurney velocity of 2700 m/s was used to estimate fragment velocities.

Two half shells were attached to each charge. For the first trial the half shells were made from 2 mm thick aluminum alloy and mild steel. The second and third trials were done with 6 mm mild steel and hard steel casings. Properties and designations of the materials are given in Table 1.

Table 1. Casing material parameters as defined in datasheets

<i>Casing</i>	<i>Hardness HV20</i>	<i>Ultimate Tensile Strength [MPa]</i>	<i>Density [g/cm³]</i>	<i>German Designation</i>
2 mm, Al-Alloy	111*	370	2.85	AlCuMgPb, 3.1645.51, F37
2 mm, Mild Steel	100-150	380-450	7.86	St 35, 1.0308
6 mm, Mild Steel	100-150	380-450	7.86	St 35, 1.0308
6 mm, Hard Steel, as received	229*	750	7.85	56NiCrMoV7, 1.2714
6 mm, Hard Steel, heat treated	484* (HV50)	1550	7.85	56NiCrMoV7, 1.2714

*measured

The test set-up is shown in Fig. 1. The charges have been point-initiated with a booster (diameter 14 mm x 15 mm) from the top. The fragments from each half shell have been recorded on three witness plates made from mild steel and having a thickness of 0.5 mm. In order to avoid excessive deformation of the witness plates they were backed by low-density foam and heavier steel plates. Holes in the witness plate caused by backsplash of fragment material from the back plate could be easily identified and were removed from the data records.

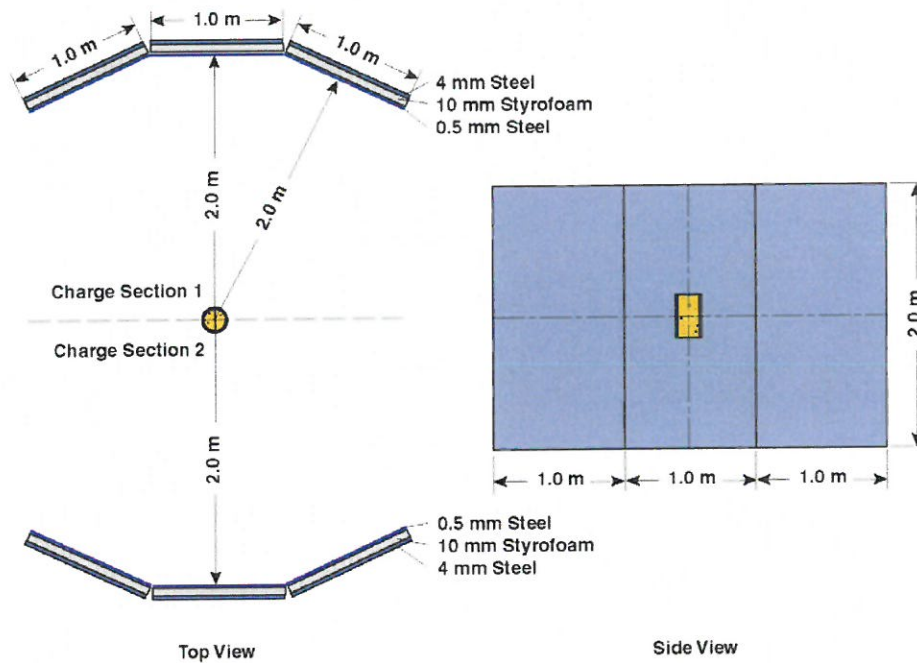


Fig. 1. Test setup with 0.5 mm steel witness plates. The charge was point-initiated from the top.

3. Data Collection Method

The applied method of data collection is based on image processing. To facilitate automatic hole detection the witness plates have to be prepared applying a definite procedure. In a first step their distortion and deformation is removed manually until an acceptably plane condition is achieved. Then the front surfaces of the plates are painted with black color and a photograph is taken with illumination from behind the plates. The effect of the preparation method is demonstrated in Fig. 2. The image obtained in this way is converted into a grayscale bitmap. Due to the high contrast of the image a simple threshold procedure is sufficient to detect the holes. Hole boundaries are stored as closed polygons and from this information the relevant data like position of the center, hole area, and orientation may be calculated. For the present purpose, namely to estimate the mass and dimensions of the fragment that pierced the hole, the hole area A_h and the length L_h and width W_h are required. Herein length and width are defined by the edges of the minimum area rectangle that contains the boundary polygon of a hole.

Determination of the fragment mass is an iterative procedure and requires some ad hoc assumptions. What we know at the outset are the initial velocity and the thickness H of a fragment. Both quantities are provided by SPLIT-X, an engineering code for the development and assessment of blast-fragmentation warheads [4]. The fragment velocity is determined by a Gurney-like method, and H is taken to be the casing thickness at breakup. The classical argument, given for example in [5], is applied to determine the state at which the casing fractures, namely when the internal pressure p equals the casing strength Y :



Fig. 2. Typical witness plate after test (left) and after preparation for evaluation (right).

$$p = Y \quad (1)$$

We take the presented area of the fragment at impact A_p as variable parameter in the iterative procedure. From the hole data we compute a form parameter λ by comparing the actual hole shape to an ellipse:

$$\lambda = \frac{A_h}{\frac{\pi}{4} W_h L_h} \quad (2)$$

Then we assume that the fragment possesses the same form factor and the same aspect as the hole, i.e. we determine the fragment width W and length L from the relations

$$\frac{L}{W} = \frac{L_h}{W_h} \quad (3)$$

$$\lambda = \frac{A_p}{\frac{\pi}{4} WL} \quad (4)$$

Since the orientation of the fragment at its impact on the witness plate is not known, we identify its actual presented area A_p with the average presented area A_c of a tumbling fragment, i.e. its so-called Cauchy-area. Then we can use the following equation to compute the volume of the fragment:

$$\frac{A_p}{V} = \frac{1}{2} \left(\frac{1}{H} + \frac{W+L}{WL} \right) \quad (5)$$

The application of this equation is justified by the fact that the equation is exact when the fragment has a rectangular shape, and that the error is less than 10% when the fragment is elliptical with $L/W < 5$. The iterative procedure to calculate the fragment mass is then given by the following steps:

- assume a presented area A_p .
- calculate the fragment mass with the help of equations (2) to (5).
- determine the impact velocity from the fragment mass, the presented area and the flight distance.
- compute the hole area as a function of the impact velocity, the presented area and material properties of the fragment and the witness plate.
- adjust A_p until the computed hole area matches the measured hole area.

Finally, since we know the total casing mass projected onto the witness plates, each fragment mass is scaled by an appropriate factor to force the cumulative mass to equal the expected mass. For the experiments described in the following paragraph the scaling was about 0.5 for the 6 mm casings and 0.8 for the 2 mm casings. This indicates that the shape of the fragments, especially of those produced by a thick casing, deviates considerably from that of a regular prism.

4. Experimental Results

Photographs of witness plates for every casing material and the two thicknesses are shown in Fig. 3 and 4. The calculated mass distributions are shown in Fig. 5 and 6. Fragment thickness, strain rate at fracture and initial velocity are given in Table 2. These quantities were estimated with SPLIT-X [4]. In addition, the number of perforations scaled up to a complete shell and the parameter β of a generalized Mott distribution of fragment masses can be found. The Mott distribution was determined by a least square fit and it has the following form

$$N \sim \left(1 - \exp \left(- \frac{m}{m_{ref}} \right)^\beta \right) \quad (6)$$

where N is the cumulative number of fragments and m is the fragment mass. The classical value $\beta = 0.5$ does not hold for the thicker steel casings. Furthermore, representing the fragmentation behavior only by the distribution function would be a poor approximation, because fragment sizes depend strongly on the axial position on the casing, which results in a non-uniform distribution on the witness plates as can be seen in Fig. 3 and Fig. 4.

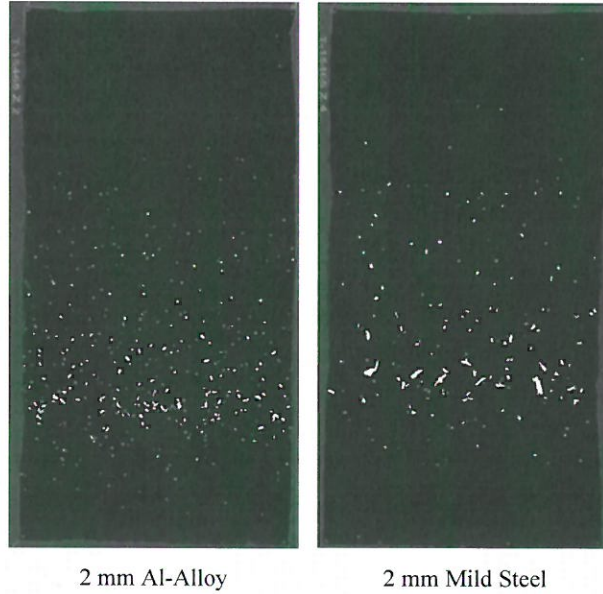


Fig. 3. Sample witness plates showing hole distributions for the two 2 mm casings.

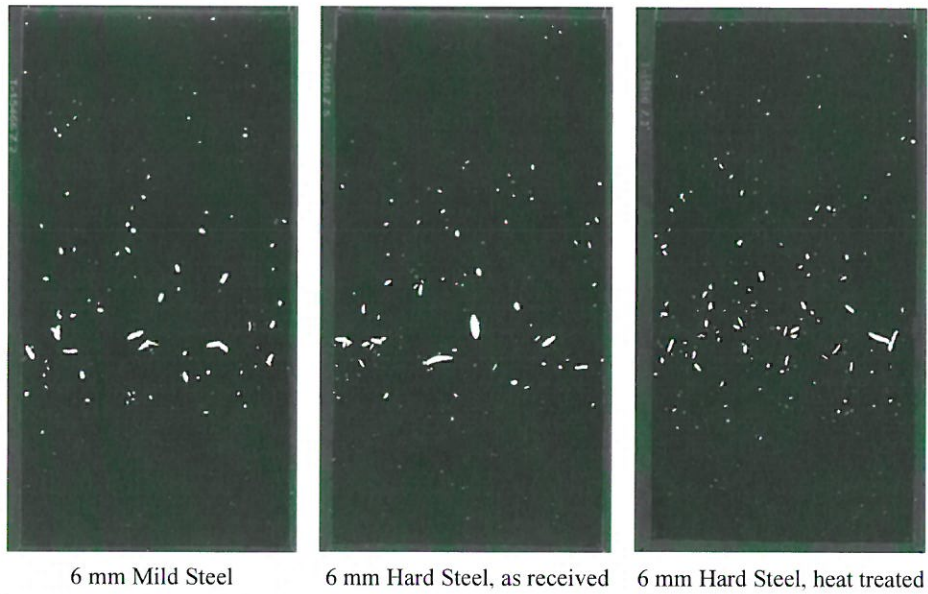


Fig. 4. Sample plates showing hole distributions for three 6 mm casings.

Table 2. Fragment mass distribution data

Casing	Total Number of Perforations	Mott Parameter β	Fragment Thickness H [mm]	Strain Rate at Fracture [1/s]	Initial Velocity [m/s]
2 mm Al-Alloy	6568	0.55	1.5	$5.0 \cdot 10^4$	3217
2 mm Mild Steel	2868	0.48	1.3	$4.0 \cdot 10^4$	2667
6 mm Mild Steel	2338	0.35	3.7	$2.7 \cdot 10^4$	1819
6 mm Hard Steel, as received	2726	0.29	4.1	$2.8 \cdot 10^4$	1819
6 mm Hard Steel, heat treated	4587	0.31	4.6	$2.9 \cdot 10^4$	1819

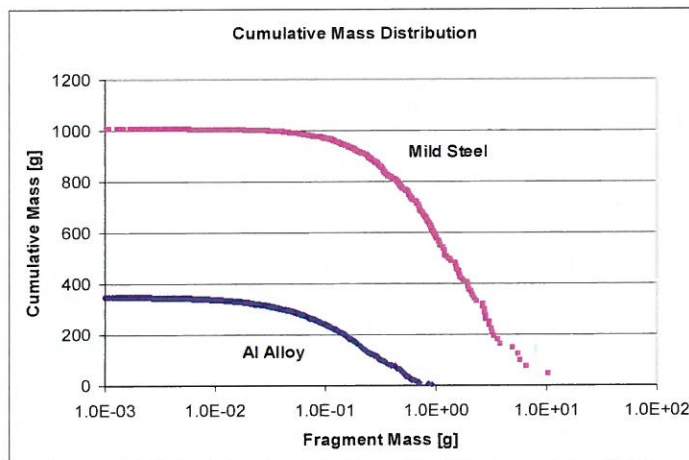


Fig. 5. Cumulative mass distributions of 2 mm Al and Steel casings.

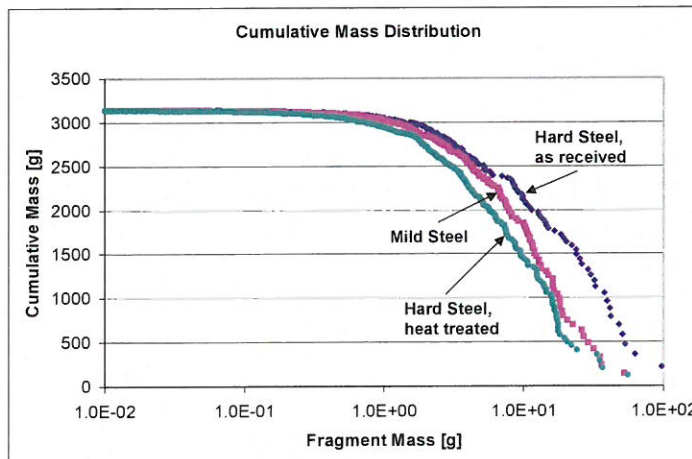


Fig. 6. Cumulative mass distributions of 6 mm steel casings.

5. Theoretical Considerations

Based on common experience it was expected that the annealed hard steel casing would produce smaller fragments when compared to the mild steel casing. Looking at Fig. 6, the opposite seems to have happened. Therefore we had to examine a known fragmentation model in more detail. The model of Grady and Hightower [5] has been developed for fragmenting steel casings of high explosive charges. Based on energy considerations the authors derived an equation for the circumferential fracture spacing, i.e. the nominal fragment width S :

$$S = \left(\frac{24\Gamma}{\rho\dot{\epsilon}^2} \right)^{\frac{1}{3}}, \quad (7)$$

where $\dot{\epsilon}$ is the strain rate, ρ is the mass density, and Γ is the fracture energy per unit area. The model considers two predominant modes of fracture in the breakup of an expanding metal shell, which are illustrated in Fig. 7. The first is tensile fracture where failure proceeds by crack propagation. This fracture mode is governed by the material's fracture toughness K_{Ic} , and an expression for the fracture energy is provided by

$$\Gamma_{\text{Tensile}} = \frac{K_{Ic}^2}{2E}, \quad (8)$$

where E is the elastic modulus of the material.

Shear fracture initiated by adiabatic shear banding is the second important mode of failure. According to [5] the shear fracture energy is given by the expression

$$\Gamma_{\text{Shear}} = \frac{\rho c}{\alpha} \left(\frac{9\rho^3 c^2 \chi^3}{Y^3 \alpha^2 \dot{\epsilon}} \right)^{\frac{1}{4}}. \quad (9)$$

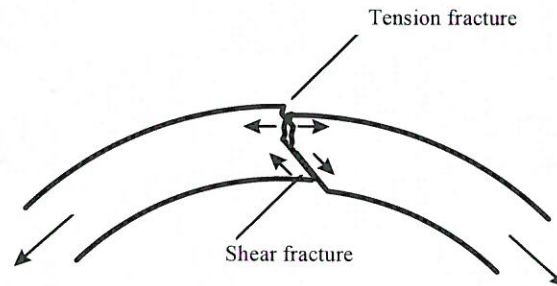


Fig. 7. Tension and shear fracture as the two basic failure modes [5].

Material properties entering this equation are the specific heat c , the thermal diffusion coefficient χ , the thermal softening coefficient α , and the plastic flow stress Y . It is empirically known that shear fracture is the dominant mode when the fracture toughness is high and the casing is not too thick. Both conditions are fulfilled for the three different 6 mm steel casings in our trials. Therefore, we can use Eqn (9) to estimate the ratio of fracture energies, and Eqn (7) to calculate the ratio of nominal fragment widths, which are shown Table 3.

Table 3. Calculated fragment widths relative to the mild steel casing

Casing	Y [MPa]	Calculated Fragment Width
6 mm Mild Steel	450	S
6 mm Hard Steel, as received	750	0.88 S
6 mm Hard Steel, heat treated	1550	0.73 S

Looking at the hole width distribution of the largest holes in Fig. 8, we indeed find slightly greater values for the mild steel in accordance with the shear fracture model. The larger fragment masses of the annealed hard steel must therefore be due to greater fragment lengths, which are confirmed by the distribution of hole lengths shown in Fig. 9. Whereas circumferential spacing, i.e. fragment width, decreases with higher material strength, this is not the case for axial spacing, where the material with the intermediate strength produces the longest fragments. The relatively low axial strain rate, especially in the central region of a detonating cylindrical shell, is probably the quantity responsible for this behavior. Consequently the shear fracture model discussed above is not applicable at low strain rates. However, to the best of our knowledge, no model is available which is adequately suited for our problem.

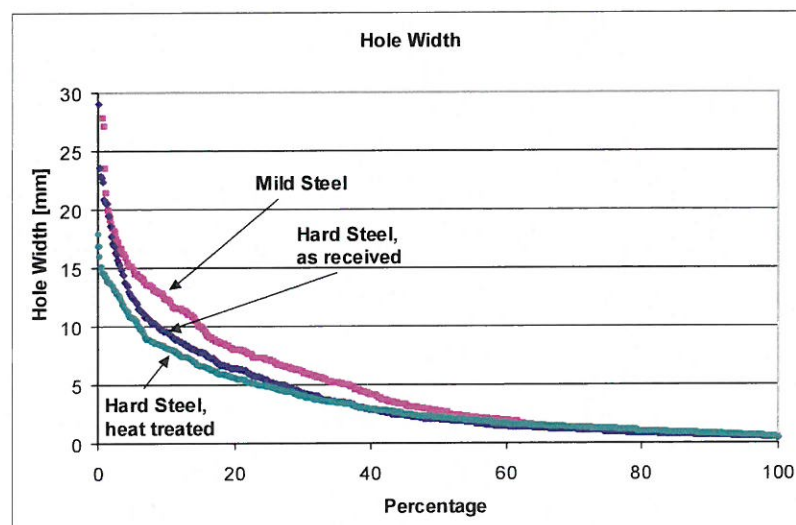


Fig. 8. Hole width of fragments from the 6mm mild and hard steel casings.

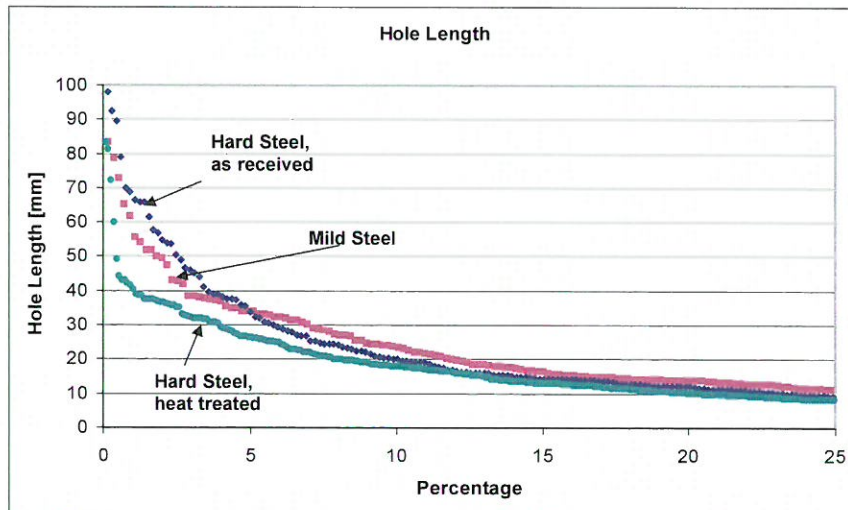


Fig. 9. Hole length of fragments from 6 mm mild and hard steel casings.

6. Conclusions

A method for fast data collection of fragmenting shells was sketched. The method was applied to generic casings of missile warheads and heavier cased ammunitions. Mass distributions gained by this method were presented for four different cases. Comparing three steel casings made of materials having different strength, we surprisingly found the largest fragments for the casing with the intermediate material strength. A closer examination revealed that fragment widths from this material were in accordance with a known fragmentation model. However in axial direction the steel casing with the intermediate strength produced the longest fragments. Development of a fragmentation model suitable for axial fracture remains a task for future activities.

References

- [1] Arnold W, Paul W. Behind armor debris investigation and their application into a New Vulnerability Model. *Int. J. Impact Eng.*, 2001; **26**: 21-32.
- [2] Arnold W, Rottenkolber E. Behind armor debris investigation (Part II). *Int. J. Impact Eng.*, 2003; **29**: 95-104.
- [3] Arnold W, Rottenkolber E. Physics of behind armor debris threat reduction *Int. J. Impact Eng.*, 2006; **33**: 53-61.
- [4] SPLIT-X, Modeling of natural fragmentation, NUMERICS GmbH, Petershausen, Germany, 2005
- [5] Grady DE, Hightower MM. Natural fragmentation of exploding cylinders, *International Conference on the Materials Effects of Shock-wave and High-strain-rate phenomena*, 1990; 713-721.

No. _____

SUPREME COURT OF THE UNITED STATES

THOMAS STALCUP,

Applicant,

v.

DEPARTMENT OF DEFENSE AGENCY,
Office of the Secretary of Defense of the United States,

Respondent.

EXHIBIT D

Thomas F. Stalcup
961 Kent Lane
Palm Harbor, FL 34683
(774) 392-0856
stalcup@gmail.com

Thomas F. Stalcup, PhD
Pro Se Litigant

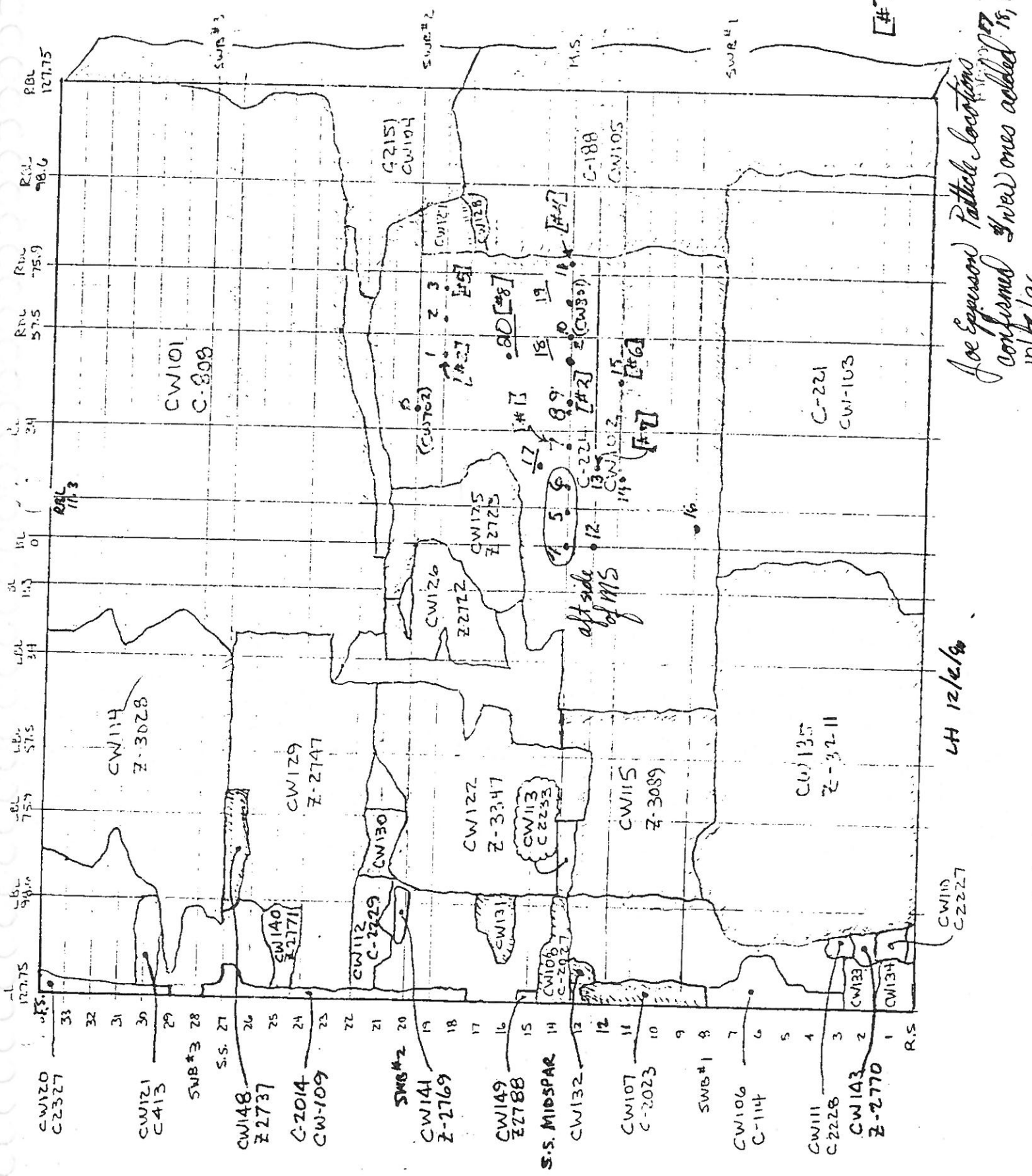
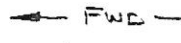
METAL PARTICLE SUMMARY

UPPER WING CENTER SECTION
SKIN PANEL

W. Stuyck

CW-102
 10/26/96
 J. TRZEL
 No. [] - NTSB SAMPLE

SUMMARY METAL PARTICLE LOCATIONS



Joe Esperson Particle Locations confirmed Good ones added 15, 19, 20 11/14/96

LH 12/2/96

METAL PARTICLE LOCATIONS
[PARTICLES ADHERING TO SEALANT
IN MOST CASES]

CW-102
10/26/96
J. TREIL

- 0 - SWBZ @ RBL 38 FRAGMENT TRAPPED IN CRACK [CW-752]
- 1 - STGR 5-19 AFT OF SWBZ @ RBL 55
[NTSB # 3]*
- 2 - STGR 5-19 @ RBL 60
3mm x 3mm
- 3 - STGR 5-19 @ RBL 70
[NTSB # 5]*
- 4 - MIDSPAR E ATTACH
- 5 - MIDSPAR @ RBL 8.94 SHEAR TIE
- 6 - MIDSPAR @ RBL 17.27 SHEAR TIE
- 7 - MIDSPAR @ RBL 31-32 [NTSB # 1]* UPPER CHORD
- 8 - MIDSPAR @ RBL 36 UPPER CHORD
- 9 - MIDSPAR @ RBL 37 UPPER CHORD [NTSB # 2]*
- 10 - MIDSPAR VERT. FLANGE @ RBL 58 TRAPPED FRAGMENT IN CRACK
[CW801]
- 11 - MIDSPAR @ RBL 79 UPPER CHORD [NTSB # 4]*
- 12 - STGR 13 @ RBL 1, 1.5, AND 3 SHEAR TIE
- 13 - STGR 13 @ RBL 22/23 [NTSB # 7]*
- 14 - CW102 @ RBL 18 AFT OF STGR 12 ABOUT 2.25 INCHES
- 15 - STGR 12 @ RBL 41/42 [NTSB # 6]*
- 16 - STGR 9 @ RBL 6/7
- 17-18-19-20 Added JE 12/4/96

* [] REMOVED BY NTSB MB 10-16-96
FOR ANALYSIS

JE 12/12/96
JE 12/17/96

CROSS REFERENCE MAP VS MARKINGS
 RE-MARKED HARDWARE ϕ -16
 METAL PARTICLE
 LOCATIONS

10/27/96
 J. TRZIL

CW-102
 10/27/96
 J. TRZIL

MAP SUMMARY
 LOCATION ITEM NO.

- ϕ
- ① NTSB # 3 ^{1/2}
- 2
- ③ NTSB # 6 ^{1/2}
- 4
- 5
- 6
- ⑦ NTSB # 1 ^{1/2}
- 8
- ⑨ NTSB # 2 ^{1/2}
- 10
- ⑪ NTSB # 4 ^{1/2}
- 12
- ⑬ NTSB # 7 ^{1/2}
- 14
- ⑮ NTSB # 6 ^{1/2}
- 16

CWT MARKINGS
 SEE NOTES FOLLOWING PAGES

①	A	FRAGMENT SCB2 @ RBL 38	} GENERALLY- WING SKIN SEALANT LINE ASSOCIATED WITH:
②	B		
A	B	} @ STGR 5-19 RBL 55, 60, 70 RESPECTIVELY	
C	C		
A	B		
B	C	} @ MID SPAR L, RBL 8.9, 17.2 RESPECTIVELY	
C	C		
F	F		
E	E	} @ MID SPAR UPPER CHORD RBL 31, 36, 37 RESPECTIVELY	
D	D		
D	D	} MID SPAR VERT FLANGE UPPER CHORD	
G	G		
E	E	MID SPAR RBL 79	
F	F	STGR 13 @ RBL 1, 1.5, 3	
G	G	STGR 13 @ RBL 22/23	
H	H	CW 102 @ RBL 18	
I	I	STGR 12 @ RBL 41/42	
		STGR 9 @ RBL 6/7	

J.E. 10/6/96
 LH 12/12/96

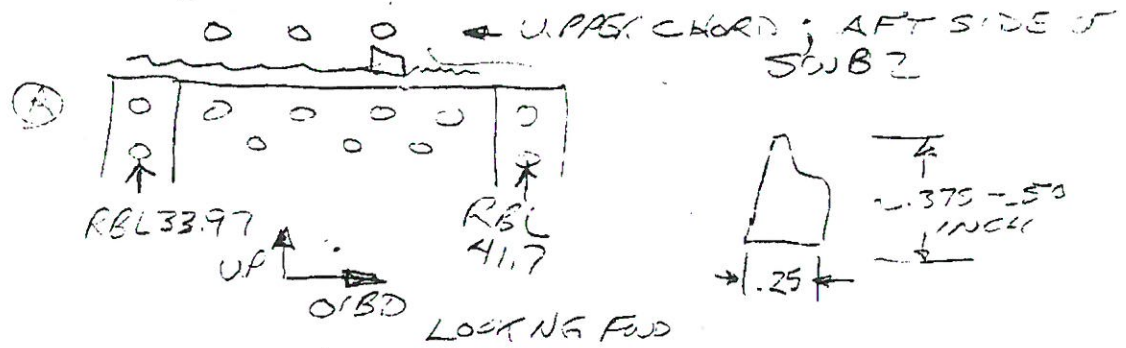
FYI -
BACK UP
ROUGH
NOTES

NOT IN
OTHER
BINDERS
LOCATION OF METALLIC
PARTICLES - SWB 2

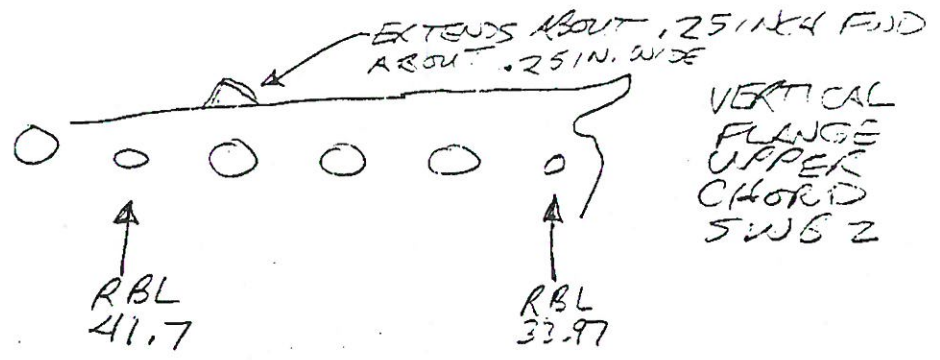
CW-702
10-26-96
J. TRZIL
(BOONIN)

Aluminum Sheet

BETWEEN RBL 33.97 & 41.7 AT ABOUT
RBL 39 A FRAGMENT OF METAL IS
TRAPPED IN A CRACK IN THE VERTICAL
FLANGE OF SPANWISE BEAM NO. 2 UPPER
CHORD



(B) LOOKING AFT



J.E. 10/6/96 (NTSB)
W 12/12/96
TWA

CENT UPPER SKIN INTERSECTION
WITH FWD MIDSPAR (S-14),
AFT SWBZ AND S-19.

CW-102
10-26-96
J. TRILL

LOCATION OF METALLIC
PARTICLES - UPPER SKIN TO
STRINGER SEALANT LINE

LOOKING
FWD

- 1 [A] STR 5-19 AFT OF SWBZ (S-20)
@ AFT SEALANT LINE WITH UPPER SKIN
@ ~RBL 55
PARTICLE REMOVED FOR ANALYSIS
BY "NTSB/MB 10/16/96 #3"
- 2 [B] STR 5-19 AFT SEALANT LINE
@ ~RBL 60
3MM X 3MM
PARTICLE - IN PLACE
AS OF THIS DATE
- 3 [C] STR 5-19 AS ABOVE EXCEPT
NEAR RBL 70
SMALL LENGTH SINGLE STRAND FINE WIRE
REMOVED BY "NTSB 10/16/96 MB #5"
FOR ANALYSIS

LOOKING
AFT

- 9: [D] MIDSPAR UPPER CHORD (S-14) FWD SEALANT
LINE NEAR RBL 37 - VISUALLY WHITE LINE
RESIDUE REMAINS AT THIS DATE
PARTICLE REMOVED FOR ANALYSIS
"NTSB MB 10/16/96 #2"
- 8 [E] SIMILAR TO [D] EXCEPT NEAR RBL 36
VISUALLY WHITE RESIDUE REMAINS AT
THIS DATE
- 7 [F] AS [D] AND [E] EXCEPT NEAR RBL 31-32
REMOVED FOR ANALYSIS BY
"NTSB MB 10/16/96 #1"
- 11 [G] AS [D] EXCEPT NEAR RBL 79
REMOVED FOR ANALYSIS BY
"NTSB/MB 10/16/96 #4"

[CW-102] CWT ^{UNDERSIDE OF} UPPER SKIN AND [CW-801] AFT MID SPAR / STG 13 / STG 12

CW-102

10/26/96

J. TRZIL

4 $\text{\textcircled{E}}$ MID SPAR $\text{\textcircled{E}}$ ATTACH LOOKING LEFT/END AT UPPER $\text{\textcircled{E}}$ SKIN UNDERTIE VARIOUS PARTICLES AND FRESH TAG AREA BY WHITE CORROSION PRODUCT

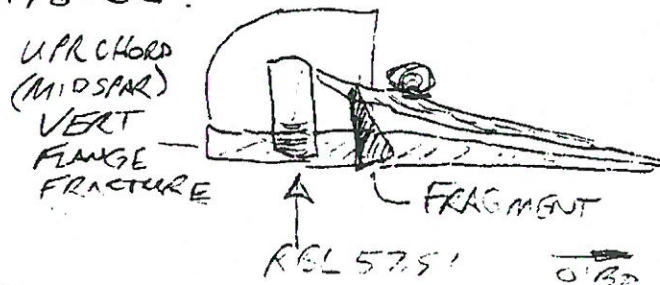
5 $\text{\textcircled{E}}$ RBL 8,94 SHEAR TIE SEALANT LINE WITH UPPER U.S. RIGHT SIDE OF SHEAR TIE VARIOUS [3 OR MORE] PARTICLES

NOTE: SOME PARTICLES ALSO ALONG SEALANT LINE BETWEEN $\text{\textcircled{E}}$ AND RBL 8,94 AFT MID SPAR UPPER CHORD TO UPPER SKIN

6 $\text{\textcircled{E}}$ RBL 17,27 SHEAR TIE SEALANT WITH UPPER STIFFENER [RIGHT O'BD CORNER LOOKING END] small slivers ~~of skin~~ - removed 10/5/96 for safe keeping

10 $\text{\textcircled{E}}$ METAL FRAGMENT TRAPPED IN CRACK SEPARATION OF MID SPAR VERTICAL FLANGE. FRAGMENT IS ABOUT 1 IN LONG (PROTRUDING AFT $\text{\textcircled{E}}$ DOWNWARDS AT ABOUT 45 DEGREES) AND ABOUT .25 INCH WIDE

CRACK PROGRESSION WAS FROM O'BD TO INSD ENDING AT SHEAR TIE LOCATION FOR RBL 57,51 STIFFENER.



ABOUT 1 INCH FROM BOLT TO FRAGMENT

Fragment matches profile of adjacent missing area of Aft flange of upper chord at crack line.

Removed for safe keeping 10/5/96

Joe Epperson NTEB

12 $\text{\textcircled{E}}$ THREE PARTICLES JUST O'BD OF SHEAR TIE $\text{\textcircled{E}}$ FOR STG 13 AT ABOUT 1, 1.5, AND 2 INCHES O'BD ON UNDERSIDE OF UPPER CWT SKIN ADHERING TO SEALANT.

13 $\text{\textcircled{E}}$ PARTICLE NEAR RBL 22/23 AT SEALANT LINE BETWEEN STG 13 AND CWT UPPER SKIN

REMOVED FOR ANALYSIS BY NTSB / MB 10/16/96 (#7)

JE 10/17/96

LOOKING END AT AFT SIDE OF MID SPAR UPPER CHORD U.S.

CWT UPPER SKIN AND
AFT MIDSPAR / STER 13 / STER 12
(CONTINUED)

CW-102
10/26/96
J. TRZIL

14 ~~14~~
No longer
Present
12/5/96 JE

METALLIC PARTICLE ADHERING TO
BOTTOM OF CWT UPPER SKIN NEAR
RBL 13 (NOTE: NOT AT SEALANT LINE)
AFT OF STER 12 ABOUT 2.25 INCHES
AND MEASURING ABOUT 2mm X 3mm.

15 ~~15~~

PARTICLE NEAR RBL 41/42 AT STER 12
AFT SEALANT LINE WITH CWT UPPER SKIN
REMOVED FOR ANALYSIS BY "NTSB MB 10/16/96" #6

16 ~~16~~
AI -
sliver JE

STER 9 AFT SEALANT LINE WITH CWT
UPPER SKIN NEAR RBL 6/7 - METALLIC PARTICLE
ABOUT 3mm X 5mm
Removed 12/5 for safe keeping.

17 - RBL 17 Red Rusty Particle - aft sealant line
1st stinger FWD of MS top skin CWT

18 RBL 44 Red Rusty discoloration in ^{aft} sealant line
of shear tie to CWT upper skin

19 RBL 67 Red Rusty spot aft sealant line
of MS upper chord

20 RBL 50 Red Rusty particle ~~made~~ on CWT
top skin under former location of 3rd stinger
FWD of MS Removed 12/5/96 JE
[NTSB #8]

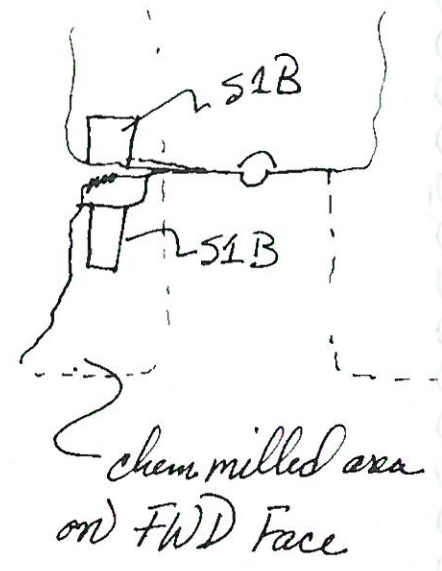
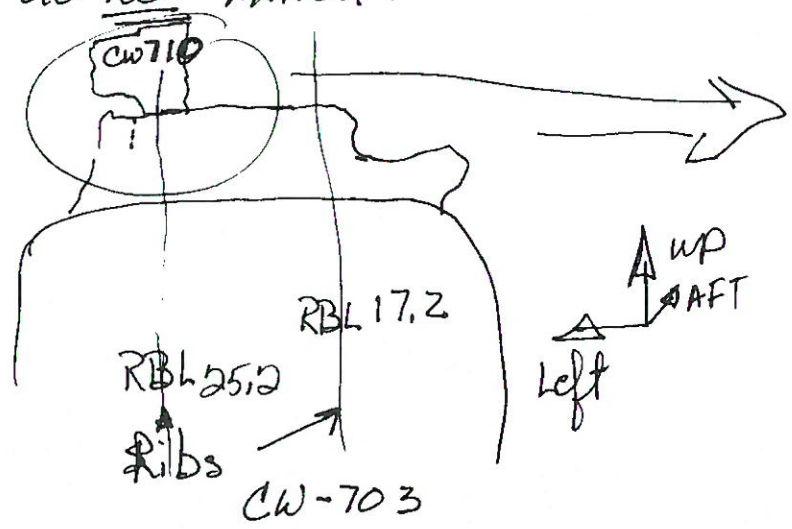
JE 12/7/96

Met Book
12/7/96
Joe Epperson
NTSB

Spanwise Beam #3 Sample (Sections)

S1T } Upper and Lower side of web above
S1B } Manufacture Door (CW-703)
Top section S1T in heated area
Bottom section S1B in non heated area

Fractures at sample locations
do not match.



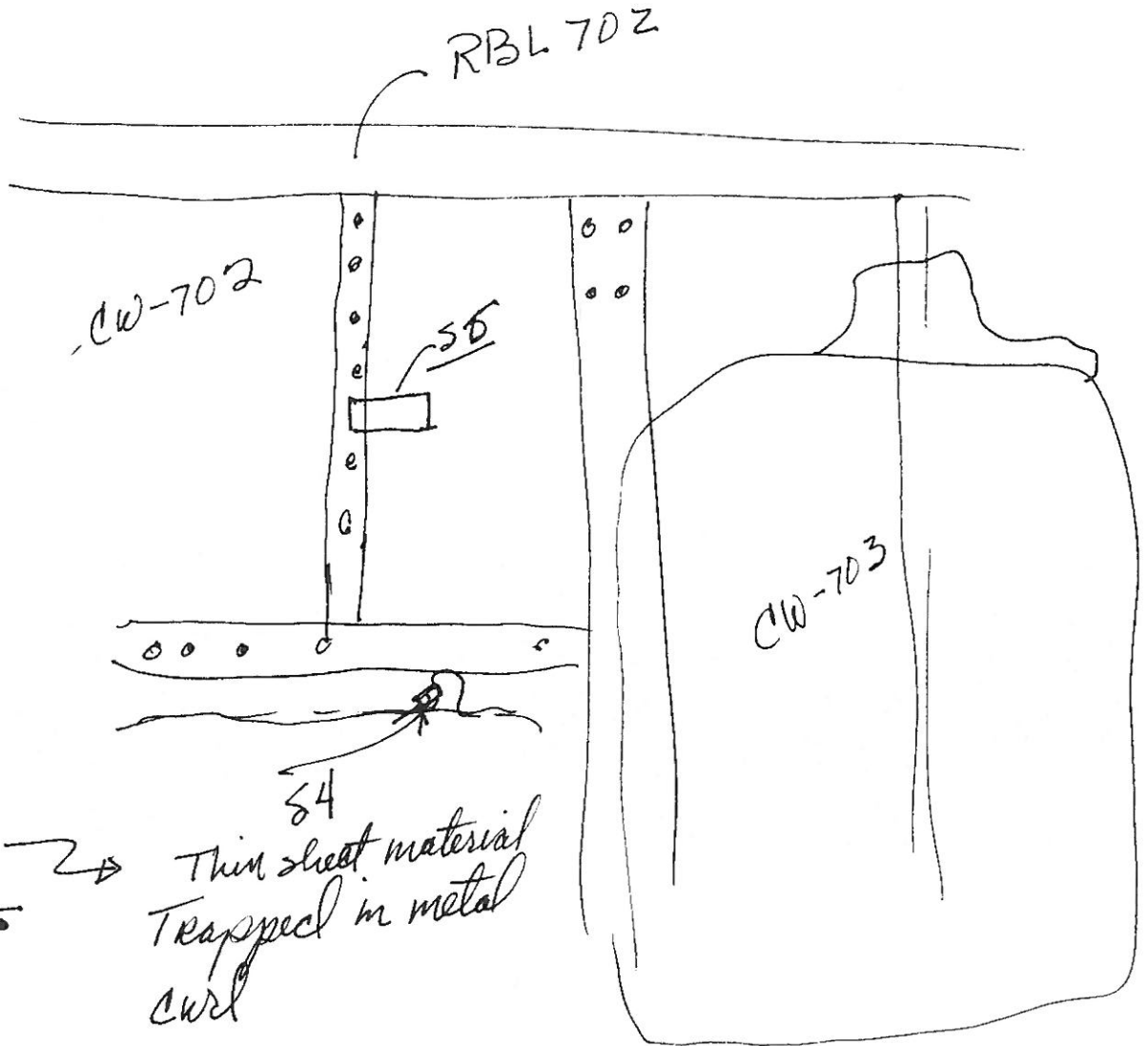
Met Book
12/7/96
Joe Epperson
NTSB

S5 → heated area horizontally across
thick area at Rib (RBL 41.7) into
thin chem milled area, to left.

SWB #3

Top bow

RBL 702



S4 → Thin sheet material
Trapped in metal
curl

NET Book
12/7/96
Joe Eppersoid
NTSB

S2 } double curled pieces
S3 } from web right of RBL 83.2 Rib
S2 midway between upper/lower chord
S3 ~~at~~ 25% up from lower chord

Markings on food face of web